

Differential Photometry for Mid to Late Type M Dwarf Stars: Determination of stellar rotational periods and comparative analysis with Radial Velocity measurements

Nicholas Kullman*
University of Missouri - Columbia

In collaboration with Dr. Andreas Seifahrt and Dr. Matt Richter

(Dated: August 19, 2010)

Abstract

Andreas Seifahrt and his team (here after referred to as Bean, et. al) have developed an ammonia absorption cell for the CRYogenic high-resolution InfraRed Echelle Spectrograph (CRIRES) at the 8m Very Large Telescope (VLT) in Cerro Paranal, Chile, and were granted a large programme with ESO to conduct radial velocity measurements on about 40 targets of mid to late type M dwarf stars. To accompany these measurements, data was also taken at the Cerro Tololo Inter-American Observatory (CTIO) on the Yale 1m telescope. Using the data obtained at CTIO, we eventually hope to obtain periodic lightcurves showing the rotational periods of our targets, possible solar spot and flare activity relative to radial velocity measurements, and resolving the degeneracy caused by the unknown value of i in $m \sin(i)$ to determine the true mass of potential planets around our targets. My primary task over the summer was to perform reduction on the data that were obtained at CTIO, and afterwards, perform aperture and differential photometry as well. At the time of writing, we are still undergoing analysis, but seem to find that very few of our selected targets showed normal periodic lightcurves.

1 Introduction

1.1 M Dwarfs

M Dwarf stars, the most abundant in our galaxy [1], are worth studying in search of extrasolar planets. These stars are classified by strong absorption bands from around 600 nm to 850 nm due to the presence of titanium oxide and vanadium dioxide [8], masses between 0.6 and 0.08 solar mass [11], low luminosity, and are relatively cool. [2] lists effective temperatures for M6 to M9.5 dwarf stars between 2800K and 2300K. Because they have such small masses, the possibility of detecting an orbiting planet around one of these stars is much higher than around solar-type stars, which are commonly the target of extrasolar planet research. The habitable zone for these planets, due to their low temperatures, is also much closer to the host star, ranging from 0.1 AU to 0.19 AU for a star with stellar mass of $0.4 M_{\odot}$ and 0.024 AU to 0.045 AU for a star of mass $0.1 M_{\odot}$, thus making the detection of a habitable planet via the radial velocity method much more likely [6]. The possibility of life on planets orbiting M dwarfs is under debate. For

an interesting argument, see [10]. Of stars of spectral class M, we are interested in studying stars of mid- to late type M, meaning that they will be on the lower end of temperature, luminosity, and mass. The targets chosen for investigation this summer were all of this type.

1.2 CCDs in Astronomy

Charge-Coupled Devices (CCDs) have revolutionized the way astronomy is performed. Compared to their predecessors such as photographic plates and solid state imaging devices, it is namely low error and their ability to achieve high levels of accuracy that make them so desirable. However, they are certainly not without complications. To understand and appreciate the data reduction that I performed this summer, it is first important to understand some basics about CCDs.

Due to the photoelectric effect, an incoming photon excites an electron on a silicon pixel in the CCD, sending it to the conduction band where it is stored on an electrode. Each pixel has its own electrode, which stores the excited electrons during the integration.

*Nick.Kullman@gmail.com

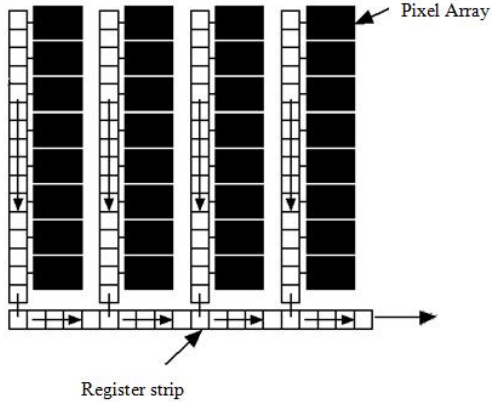


Figure 1: *Pixel readout on a CCD occurs in a row-by-row fashion. Once a row is moved onto the register strip, the on-chip amplification and analog-to-digital conversion occur before saving the data.*

The ratio of photon hits to collected electrons is essentially one; however, this is only true up to a certain point. For common astronomical-use CCDs, linearity will generally last to around 50,000 counts. Pixels with counts greater than the linearity limit of the CCD are unreliable and can often cause 'bleeding', or the overflow of electrons into neighboring pixels. This effect can ruin an integration. After the integration is complete, the CCD is read out in a row-by-row manner as seen in Figure 1.

This is the first source of instrumental error. Every time a charge is transferred during read out from one pixel to the next, only a certain percentage is actually transferred from what was collected. This number is called the quantum efficiency (QE) of the device and for modern CCDs is typically near 99.9999% [5]. Once transferred, the voltage obtained by each pixel is read out by an analog-to-digital converter, which assigns a numeric value corresponding to the voltage (a so-called 'digital number' (DN)), and then amplified before either being saved or transferred to another machine that will interpret these values (as an image, per se).

The second primary source of error for a CCD is the dark current, which is caused by thermal generation of electrons within the CCD. This is an intrinsic and inevitable source of error in a CCD, but can be significantly decreased with cooling of the device. In addition to the dark current, other intrinsic sources of error are bad or 'hot' pixels on the array, the QE of each pixel, the amplification of the voltage during readout, and the analog-to-digital conversion, among others. There are methods to minimize and eliminate these errors, and this is discussed in Section III of this

letter.

1.3 Radial Velocity Measurements

The first confirmed detection of an extrasolar planet was in 1992, and the number of confirmed discoveries has been growing exponentially ever since. Up until recently (with the disclosure of the success of NASA's Kepler mission), the most common form of detection was through radial velocity measurements (Kepler uses the transit method—see below). The radial velocity method consists of collecting the radiation from a target (generally within a specific band), performing high-resolution spectroscopy, and analyzing shifts and distortions in the stellar spectrum. The light from the source is passed through a cell, which creates a 'picket fence' background to which the observer can compare the stellar spectrum. Typically, the cell used is filled with iodine, which provides many deep, narrow absorption lines in the visible spectrum. From observing the shifts and distortions in stellar spectra over time, certain parameters can be deduced. The translational velocity of the star along the line of sight to the observer (radial velocity), the planet's distance from the star, its minimum mass, velocity of both bodies, and more can be found. The rotational velocity can be inferred by high resolution spectroscopy as well. When a planet rotates, as long as it is not pole-on to the observer, a simultaneous redshift and blueshift is observed. This effect occurs because during rotation, one side of the planet is rotating away from the observer while the other is rotating towards them. This effect does not cause a translational shift of the spectral lines, but rather a blurring or widening. The effect hinders the precision of radial velocity measurements, and thus the rotational period of stars is studied by other means, such as differential photometry, in attempt to resolve this error. Observations over time will provide the data necessary to determine a period for the object. Although generally the period describes the gravitational wobble of the star due to an orbiting body, this is not always the case, and determining the exact meaning of this derived period is part of our investigation.

1.4 Photometry

There are two broad photometric methods of collecting data on stellar objects, mainly absolute photometry and differential photometry. Absolute photometry attempts to observe the true brightness of an object, while differential photometry is a measurement of the brightness of an object relative to others in the same field. Absolute photometry is ideal, however in ground-based observations this method is generally not achievable. Differential photometry is the most

accurate and practical method, achieving errors as low as This summer we employed the differential photometry method. It is done by calculating a target's flux relative to other comparison stars in the field. See [3] for a more rigorous description of differential photometry, its advantages, and the determination of comparison stars.

1.4.1 Aperture Photometry

Aperture photometry is a means of measuring the flux of a selected body. It consists of encircling the body with a circle (aperture) of radius r , an inner sky annulus of radius $a(i)$, and an outer sky annulus of radius $a(o)$ (Note: $r < a(i) < a(o)$). The disk with inner radius $a(i)$ and outer radius $a(o)$ serves to measure the background flux from the sky, while the circle of radius r immediately around the target measures its flux above the background.

1.4.2 Transit Studies

A transiting planet is one whose orbit passes between its host star and an observer. The transit method of extrasolar planet detection involves studying the flux from a target as it passes in front of its host star. Given a sampling of the flux level from the target, when a planet passes in front of it, there will be a noticeable decrease in the measured flux. The decrease in flux is equal to the ratio of the relative surface areas of the planet and the host star. A planet detected using this method must always be confirmed by another method, typically by radial velocity measurements. Likewise, radial velocity detections may be followed up by photometric methods in the chance of detecting a possible transit. The transit method is the most revealing of a planet's characteristics, as it can be used to deduce the planet's true mass, the chemical composition of its upper atmosphere, its temperature, density and more.

2 Methods

The iodine absorption cell mentioned in Section II.iii works well for observations taken in the visible spectrum, but fails when approaching the near infrared. Our targets were mid to late type M dwarf stars, which produce strong absorption bands from 600 nm to 850 nm [8], thus reducing the usefulness of this particular cell. Instead, Bean et al. developed a quartz ammonia gas cell which allows this same strategy to be performed in the near infrared. Bean et al. were granted an ESO Large Programme to allow for the study of about 40 mid- to late type M dwarfs which they did using their new ammonia gas cell with CRIRES on the VLT in Chile. To accompany these

measurements, more data were desired to: 1) Rule out false positives in radial velocity detections, 2) Determine an extrasolar planet's true mass rather than just the $m \cdot \sin(i)$ obtainable from the radial velocity measurements, and 3) To study the correlation between stellar activity and radial velocity in the optical and infrared. To obtain this data, observations were done at the CTIO Yale 1m telescope, and this is the data I worked with this summer.

2.1 The CCD on the Yale 1m

The CCD on the Yale 1m at CTIO is the Y4KCam 4Kx4K. The Y4K cam is a 4104x4104 pixel array, with an overscan cross of width 40 pixels, thus making the final image size 4064x4064. It is linear within 1% up to 42,000 counts above the bias, has a gain of 1.4 electrons per digital number, a full-well capacity of 66,000 electrons, and has a field of view of 20 arcminutes by 20 arcminutes. The very beginning of my summer was spent investigating the importance of these values and of CCDs in astronomy as well.

2.2 Data Reduction

2.2.1 Creating a Master Bias

Once given the raw data, I was introduced to Interactive Data Language (IDL), an array based program widely used in astronomy. Using IDL, my first task was creating a bias file to be used for each night's observations. A bias frame is created by taking performing an integration of 0 seconds with the shutter closed. This process gives you the 'zero image' of the CCD, made up of dark current effects and read out errors. A series of bias frames are taken at the beginning and the end of each night of integration to account for slight fluctuations in the zero image error sources, and a master bias is computed from these frames. The master bias frame is created by computing a sigma-clipped mean over the stack of bias frames taken during the night once the error-ridden bias frames are excluded from the data set. Once this master bias is created, it is subtracted from all other frames for the corresponding night.

2.2.2 Creating a Master Flat Frame

The next step in data reduction is generating a master flat field image by which all images will be divided. The purpose of this image is to eliminate errors caused by fluctuations between individual pixels' readouts, gains, and quantum efficiencies. The idea of a flat field is to expose the CCD to a spectrally and spatially flat source that would in theory register an equal response from each pixel [5]. Since the

pixels on the CCD react differently to different wavelengths of light, a series of flat field images must be taken for each filter that is to be used during the observation. Flat fields are normally obtained in one of two ways. The first way is through observing a special screen located within the telescope dome('dome flats'), and the other is by taking observations of the twilight or night sky ('sky flats'). Sky flats were used in our observations, and they were taken at the beginning and end of each night of observation (pre- and post-observation flats). Before flat fields can be applied to images, they first need to be corrected themselves. This includes normalization for all flats, and for flats with integration times less than or equal to 3 seconds, corrected for distortions from the shutter as well. For longer integrations, the effects of varying brightness due to the shutter speed are negligible. After being normalized and shutter-corrected, due to filters and lenses that were not kept under vacuum, new dust specs frequently appeared in our images. Hence, in our case, we also had to analyze each individual flat frame for inconsistencies between it and the prior flat. Where two consecutive flats showed noticeable inconsistencies, a note was made and the division for groups of flats to create a master flat was established in these gaps. Typically two master flats were produced for each night of observation—one from the pre-observation flat fields, and the other from post-observation.

2.2.3 Image-Specific Determination of Appropriate Flat

Once master flats had been created, the pre-observation master flat was applied to all science frames from that night. The science frames were then analyzed to determine whether the pre- or post-observation flat resulted in a better image. Figures 2 and 3 show a corrected science frame, first with the incorrect choice of a master flat, and then with the correct choice.

Once the appropriate master flat had been chosen for each image, the central overscan cross was removed from all science frames.

2.2.4 Target Location

After all science frames had been corrected, the target had to be located in each image and its pixel coordinates recorded. There is no automated way of performing this task. The process of determining which star in our fields was the target required the use of a program called Aladin Sky Atlas. Aladin allows the user to enter the name of their target and select which past sky surveys they would like to use images from in determining the location of the target. By the user-performed process of correctly orienting the images

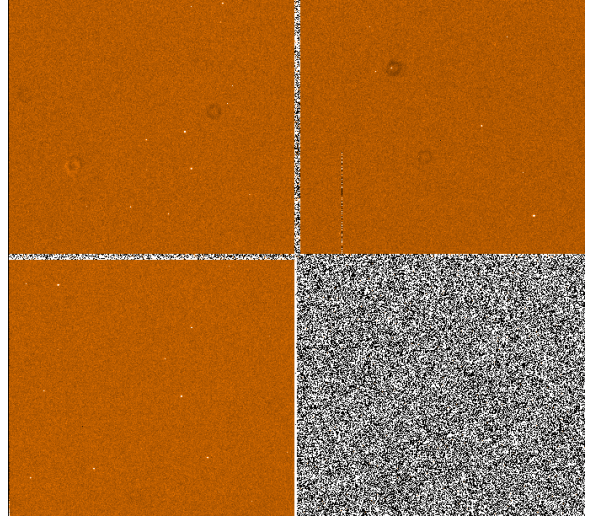


Figure 2: Science frame taken at CTIO on Yale 1m telescope using an incorrect flat field correction.

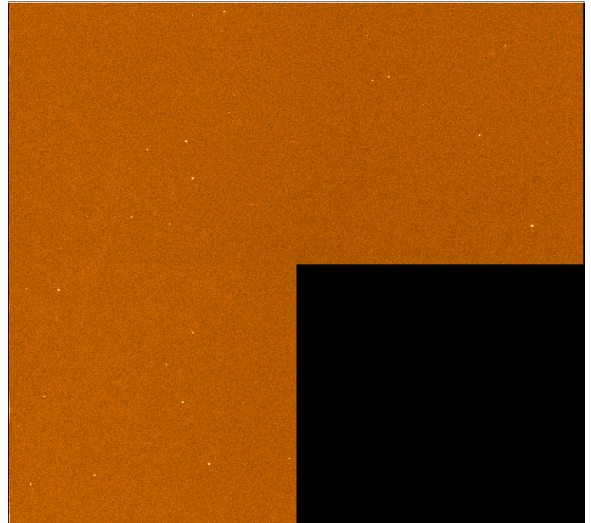


Figure 3: Same science frame as in Figure 2 but with the proper flat field correction.

and doing scrupulous image comparison, finding the target can be done by employing a sort of "Where's Waldo" method.

2.2.5 Star Detection within Science Frames

Within IDL, the program FIND is able to detect the presence of bright objects in an image. Since the sky generates a background value for every pixel, FIND first computes the median sky value and subtracts it from the image. FIND then scans the image for brightness perturbations, uses marginal Gaussian fits to find centroids, and computes 'roundness' and 'sharpness' values of the detected objects. The roundness refers to the elongation of the object, whereas the sharpness refers to the steepness of the Gaussian used to fit the object. The user can enter preferred roundness and sharpness criteria that will assist in the removal of false detections of stars, such as in hot pixels or galaxies. FIND returns a list of the stars detected in the image, their x and y pixel coordinates, the number of counts for each star, and their sharpness and roundness values. The output is such that it is easily read into the program APER.

2.3 Aperture Photometry

Next, a program called APER performs aperture photometry on the objects supplied in the user-given input list, which were in our case obtained from FIND. APER is capable of performing aperture photometry for up to 12 given aperture radii. For our measurements, APER was run with aperture radii of 7, 10, 12, and 14 pixels. As output, APER produces a file containing an array which has for each star its x and y pixel coordinates and the flux for each supplied aperture radius. With multiple observations for each target, the files produced by APER were sorted into lists, one per target. These lists were then run through a program created by Andreas Seifahrt to create files readable by Chris Broeg's dphot program. In addition to petty formatting issues that had to be resolved, the more serious problem with aper results was that for the same target, depending on the pointing of the telescope, the comparison stars in the images will not always be the same. This issue was resolved by a robust technique in a program developed by Seifahrt called matchlists.pro. In this program, the distance from every star in the field to every other star is computed, and histograms made showing the hits for these distances along the x and y directions. Except for in very sparse fields or extremely dense fields, there always existed a clear peak in the histogram. For each pair of aper files within a target's list, this distance was recorded as the offset between the images. Using this offset and the program create_magfiles.pro, a list of common comparison stars

from all files can be determined. This program produces mag files containing the flux, julian date, and error for each comparison star.

2.4 Differential Photometry

Using the output mag files from Seifahrt's create_magfiles program, Chris Broeg's dphot program is called. This program performs differential photometry, weighing the comparison stars in such a way that their error is minimized [3]. For a detailed description of the weight calculations used and the means of determining differential magnitudes see Broeg, et al, 2005.

2.5 Lightcurves and Determining Periods

The differential magnitudes and associated errors calculated by dphot were then plotted in IDL as lightcurves, one for each of our targets. A lightcurve shows the differential flux measured over time. These are the true results that we hoped to obtain from day one. Thus far, two methods have been used to analyze the results seen in these lightcurves. For lightcurves of our targets, see figures in Results & Conclusions below.

2.5.1 Lomb-Scargle Periodogram

As our data is unevenly sampled (6 integrations per target per night), each target's lightcurve is a series of points with gaps of roughly one day in between observations as seen in the lightcurves displayed below. The IDL program scargle.pro computes the Lomb-Scargle periodogram for unevenly sampled data. For the details on this calculation, see Scargle, 1982 and Horne & Baliunas, 1986.

2.5.2 Period04

The second means of extracting periods from our lightcurves was using the program Period04. Produced by Delta Scuti Network, it is designed to perform Fourier analysis of unevenly sampled data and extract the most prominent frequencies.

3 Results & Conclusions

Four targets of our 25 selected will receive mention in this letter. The first is LHS2065 whose lightcurve can be seen in Figure 4 below. Within error, this target seemed to show very stable radiation in R over the course of our observations except for during the fourth night. Martin & Ardila, 2001 note that this M9 star with mass between 0.1 and 0.06 $M_{(sun)}$ shows microflare activity at the rate of 0.5 microflares hr^{-1} .

They also note that strong flare activity is rare (0.03 strong solar flares hr^{-1}). With this information, it is possible that the increase in differential magnitude that we witness on the fourth night is due to the star's microflare activity.

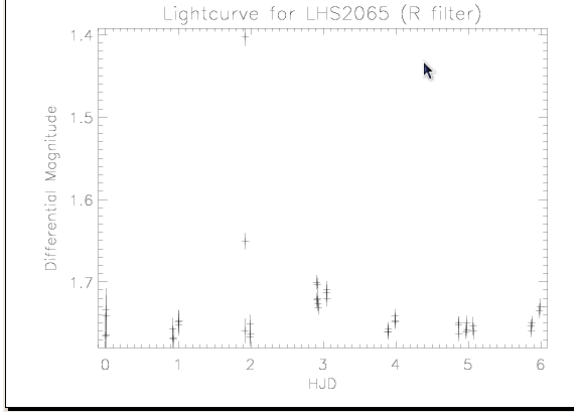


Figure 4: *Lightcurve obtained from target LHS2065, an active M9 star. The middle night shows possible microflare activity.*

The second and third targets are GJ300 and LHS3003 (see Figures 5 and 6). Based upon our data, both targets appear to be very quiet with little stellar activity (standard deviation of differential magnitude of only 0.00485165).

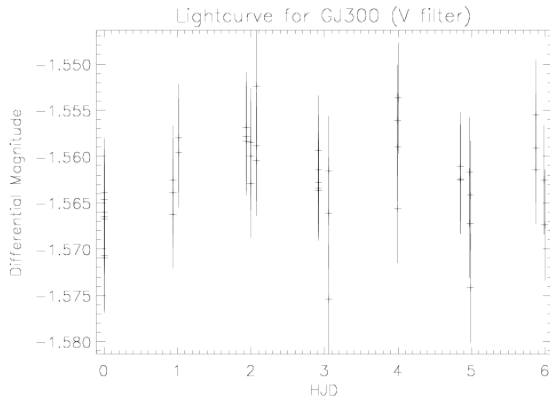


Figure 5: *Lightcurve obtained from target GJ300. Flat lightcurve suggests very little activity with the standard deviation of its differential magnitude at 0.00485165 .*

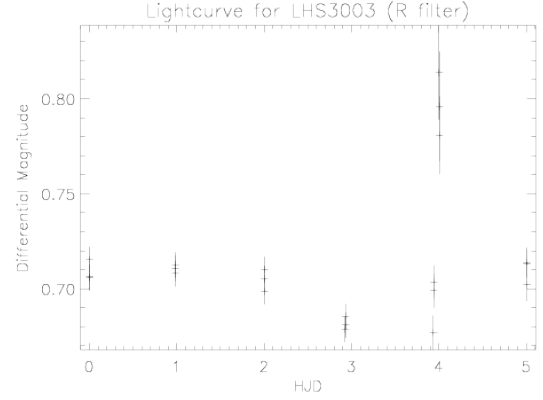


Figure 6: *Lightcurve obtained from target LHS3003. Again, its flat lightcurve suggests very little activity with data problems in the second to last night.*

Finally, SO053 appears to show periodic tendencies; however, our observations of this target were not long enough to capture a full period, though it appears to have a period of 5 days (see Figure 7). It would be worthwhile to perform a follow up observation of this target to get a better measure of its period.

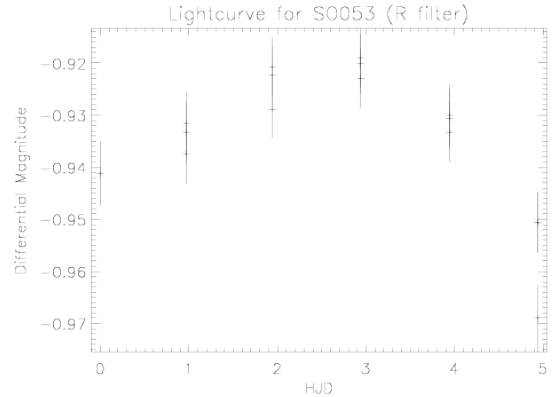


Figure 7: *Lightcurve for target SO053. While it appears to show a period of 5 days, our observations were not long enough to say this with certainty.*

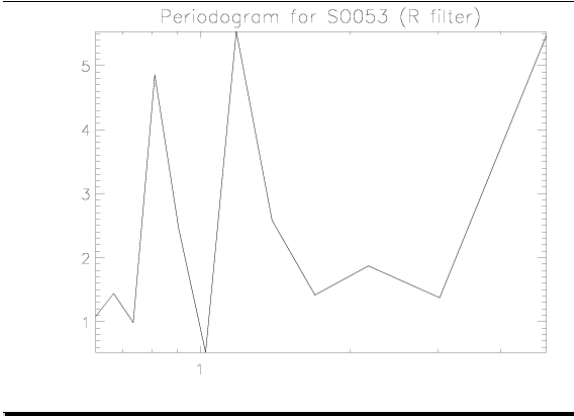


Figure 8: Periodogram for target SO053, showing two false peaks from our window function. Comparing the lightcurve and periodogram information, the spike that appears to be rising at 5 days hints at a true period corresponding to this time, but additional observations are necessary to confirm.

The majority of the remainder of our targets showed lightcurves that were not periodic in nature. Examples of DENIS1048 and GJ1156 are shown below.

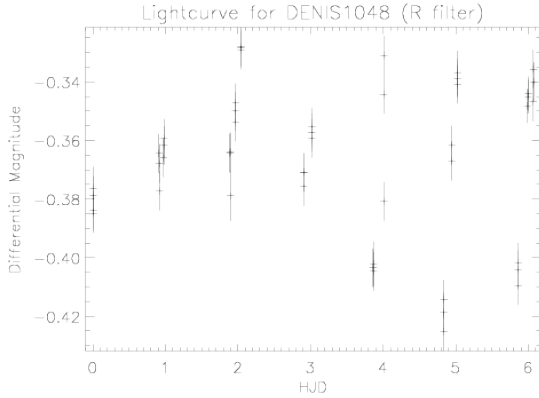


Figure 9: Lightcurve for target DENIS1048. As is apparent, this lightcurve is very noisy; no rotational period was able to be derived from this data.

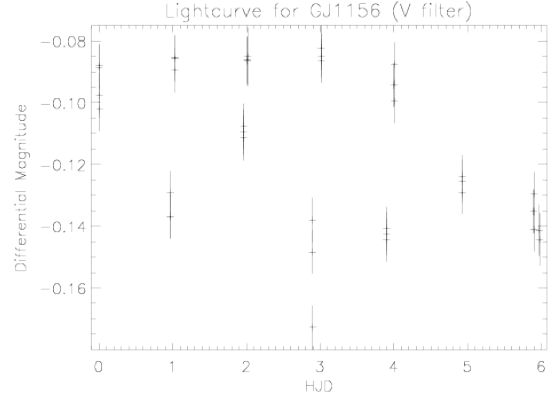


Figure 10: Lightcurve for target GJ1156. Similar to DENIS1048, with the noise in the lightcurve no direct period determination was possible from our methods.

Table 1 shows the standard deviation of the differential magnitudes as well as the mean error for each target. The results of this table tell us that although our lightcurves were very noisy, in most cases this is not due to a lack of precision in our measurements. This points to possible signal activity causing these values, but certainly needs to be confirmed.

TARGET	σ (dmag)	Mean uncertainty
DENIS1048	0.02585510	0.00665416
G099_049	0.01636940	0.00583265
GJ54_1	0.02417420	0.00869167
GJ285	0.02125740	0.00621346
GJ299	0.01210400	0.00585745
GJ300	0.00485165	0.00586444
GJ388	0.01675480	0.00825000
GJ406	0.01602470	0.00613514
GJ551	0.00853264	0.00605962
GJ644C	0.02707370	0.01402220
GJ1057	0.00588955	0.00616944
GJ1061	0.00993391	0.00586512
GJ1093	0.01361240	0.00744285
GJ1128	0.01069410	0.00683902
GJ1154	0.01178630	0.00620357
GJ1156	0.02550670	0.00732778
LHS288	0.00902781	0.00580000
LHS292	0.02619190	0.01167390
LHS337	0.02071600	0.00561143
LHS1723	0.00579909	0.00578039
LHS2065	0.01852420	0.01148330
LHS3003	0.03647890	0.00983810
LP944_20	0.01684680	0.01183560
SIP1259	0.01224670	0.00818276
SO053	0.01353580	0.00581875

Table showing the standard deviation of the differential magnitude of each target along with its mean uncertainty. The data in the table suggests that the noise seen in most lightcurves may actually be due to activity signals.

4 Future Research

More extensive observation of our targets that appear to show longer periods would be a worthwhile task to provide more certain data to accompany the radial velocity measurements taken with CRIRES on the VLT. In addition, the data from the VLT could be used to selectively pick a smaller subset of these targets which currently show signals in the radial velocity measurements. By observing a smaller set of targets over a longer time scale (both in number of nights and also observations per target per night) better lightcurves would be obtained, more rotational periods could be measured, and stellar activity would be more evident.

References

- [1] Bean, J. et al. (2010) *The CRIRES Search for Planets Around the Lowest-Mass Stars. I. High-Precision Near-Infrared Radial Velocities with an Ammonia Gas Cell*. The Astrophysical Journal, (713), 410.
- [2] Basri, G. et al. (2000) *An Effective Temperature Scale for Late-M and L Dwarfs, from Resonance Absorption Lines of Cs I and Rb I*. The Astrophysical Journal, (538), 363-385.
- [3] Broeg, C. et al. (2005) *A new algorithm for differential photometry: computing an optimum artificial comparison star*. Astronomische Nachrichten, (326), 134142.
- [4] Horne, J. & Baliunas, S. (1986) *A Prescription for Period Analysis of Unevenly Sampled Time Series*. The Astrophysical Journal, (302), 757-763.
- [5] Howell, Steve B. (2006) *Handbook of CCD Astronomy*. Cambridge University Press, 2nd edition
- [6] Mandell A, Raymond S, Sigurdsson S. (2007) *Formation of Earth-like planets during and after giant planet migration*. Astrophysical Journal, (660), 823-844.
- [7] Martin, E. & Ardila, D. (2001) *Flares at the Cool End of the M Dwarfs: The case of LHS2065*. The Astronomical Journal, (121), 2758-2760.
- [8] Reid, Neill. (2002) *Spectral Classification of late-type dwarfs*. <http://www-int.stsci.edu/inr/ldwarf.html>
- [9] Scargle, J. D. (1982) *Studies in astronomical time series analysis. II - Statistical aspects of spectral analysis of unevenly spaced data*. Astrophysical Journal, (263), 835-853.
- [10] Tarter, J.C., et al. (2007) *Special Paper: A Reappraisal of the Habitability of Planets Around M Dwarf Stars*. ASTROBIOLOGY, Volume 7, Number 1.
- [11] *Red Dwarf Star*. McGraw-Hill Encyclopedia of Science and Technology, 5th edition, 2009.

This research has made use of the SIMBAD database, operated at CDS, Strasbourg, France.
This research has made use of Aladin.